PHYSICSAccess Research Paper
ISSN Online: 2756-3898, ISSN Print: 2714-500X https://doi.org/10.47514/phyaccess.2024.4.1.004

Ultra-Thin 2D $MoTe_2$ for Electron Transport Material Application in Perovskite Solar Cell: A Theoretical Approach

Mohammed Adamu[1], Shuaibu Alhassan[1], Sadiq G Abdu[1] and Muhammed M Aliyu[1]

[1] Department of Physics, Kaduna State University, Kaduna PMB 2339, Kaduna, Nigeria

Corresponding E-mail: adamu.mohammed@kasu.edu.ng

Received 28-03-2024
Accepted for publication 30-04-2024
Published 02-05-2024

Abstract

With rapid progress in power conversion efficiencies, perovskite solar cells (PSCs) have shown great potential as next-generation low-cost, efficient solar cell devices. Ultra-thin pure and Br-doped $MoTe_2$ monolayer materials are promising candidates for alternative electron transport material in perovskite solar cell applications. The electronic, and optical properties of these materials were calculated using projector augmented plane wave (PAW) based on popular density-functional theory (DFT). These properties were calculated using Pardew-Burke-Ernzerhof generalized gradient approximation (PBE-GGA). The band structure for the considered materials has been determined using full relativistic spin-orbital coupling (SOC). Our results indicate that pure and Br-doped 2D-$MoTe_2$ were n-type semiconductors and had direct band gap energies of 1.01 and 1.21 eV respectively. The optical properties of the materials such as relative dielectric constant, transmission and reflectivity are presented. Using these properties, the 1-D solar cell capacitance simulator (SCAPS-1D) software was used to design solar cells based on monolayer pure and Br-doped $MoTe_2$ as an electron transport layer (ETL). The maximum efficiencies of these cells are 13.121%, and 24.016% with V_{OC} of 1.067 V and 1.186 V, J_{SC} of 21.678 mA/cm^2 and 25.251 mA/cm^2, and FF of 56.720% and 80.139% were realized with the pure and Br-doped ETLs respectively. The performance of our solar cells is comparable to traditional Si-based solar cells. The results show how monolayer pure and Br-doped $MoTe_2$ can serve as a suitable ETL material for perovskite solar cells.

Keywords: DFT; SCAPS-1D; Perovskite solar cell; 2D-$MoTe_2$; Electron transport material.

I. Introduction

Solar energy has been the most important and environmentally friendly among all other sources of electrical energy [1]. A large amount of this energy falls on the surface of the earth every day. Solar cells are one of the technologies used to convert solar radiation to electrical energy for human survival [2].

Perovskite solar cells (PSC) have drawn a lot of attention due to their high power conversion efficiency (PCE) of more than 25% [3-5]. The device is composed of perovskite material inserted between two charge carrier layered materials namely the electron transport and hole transport materials [6, 7] (Fig. 2b). The electron transport layer (ETL) extracts electrons from the perovskite light absorber and transports them to the cathode, at the same time it blocks holes from reaching the cathode of the cell. While the hole transport layer (HTL) did the reverse with respect to the anode. The ETL plays a

significant role in determining the power conversion efficiency of the device [8-10]. Therefore, the selection of better material for ETL has become very crucial.

For the absorption layer, Methylammonium lead triiodide ($CH_3NH_3PbI_3$ or $MAPbI_3$) is considered for this work for its good physical properties, such as excellent absorption coefficient, high diffusion length, low exciton binding energy, prolonged carrier lifetime and variable band gap energy [11]. Though the material is moisture sensitive and due to lead content, it is considered poisonous to the environment. However, on the issue of moisture, a few years back a flouropolymeric coating was employed to encapsulate the material. This technique is reported to be effective since the tested cell retains 95% of its initial PCE after working for 92 days [12]. On the issue of lead, some lead-free halide perovskites have been developed such as $MASnI_3$. Even though, these perovskites have shown poor performance compared to the $MAPbI_3$[13]. Further, it has been reported that the lead content in the ultra-thin film of $MAPbI_3$ is insignificant to have any environmental impact [14].

Two-dimensional Transition Metal Dichalcogenides (TMDCs) have attracted tremendous attention from researchers most especially in optoelectronic devices [15-17]. These materials are generally represented by a formula given by MX_2, where M is transition metal (Group iv to xii of the periodic table) and X is Chalcogens (S, Se, Te) [18]. A metal is sandwiched between two chalcogens. The interatomic force is covalent while the interlayer is Van der Waals in nature [19]. These materials are characterized by having promising electronic and optical properties for application in photovoltaics [20, 21]. Doping of appropriate atoms into TMDCs can enhance the electronic and optical properties of the material significantly [18]. It has been reported by many researchers that doped ETL materials are promising for improving solar cell performance [9, 22-26]. Due to the absence of dangling bonds, high electron mobility, high conductivity, and high transparency in the visible spectrum, doped and pure $MoTe_2$ monolayers could be better than the commonly used ETL materials such as TiO_2, SnO_2, and ZnO [8]. This could potentially serve as ETL in more flexible and lightweight photovoltaic panels. In this perspective, Alzaid [27] and Ahmad et al [28] specifically pointed at the 2D-$MoTe_2$ material for use as ETL in PSC.

Just like many other two-dimensional di-chalcogenides, 2D-$MoTe_2$ is three atoms thick [19], a sheet of Mo atoms sandwiched between two sheets of Te atoms, making a monolayer (Fig. 1). Their unique structural, electrical and optical properties make them different from their bulk (Fig. 1) counterparts and appealing for use in Photovoltaic. Moreover, the ultrathin structure makes this material inherently flexible, and almost transparent which are required properties for lightweight, flexible, wearable and building integrated solar modules [29].

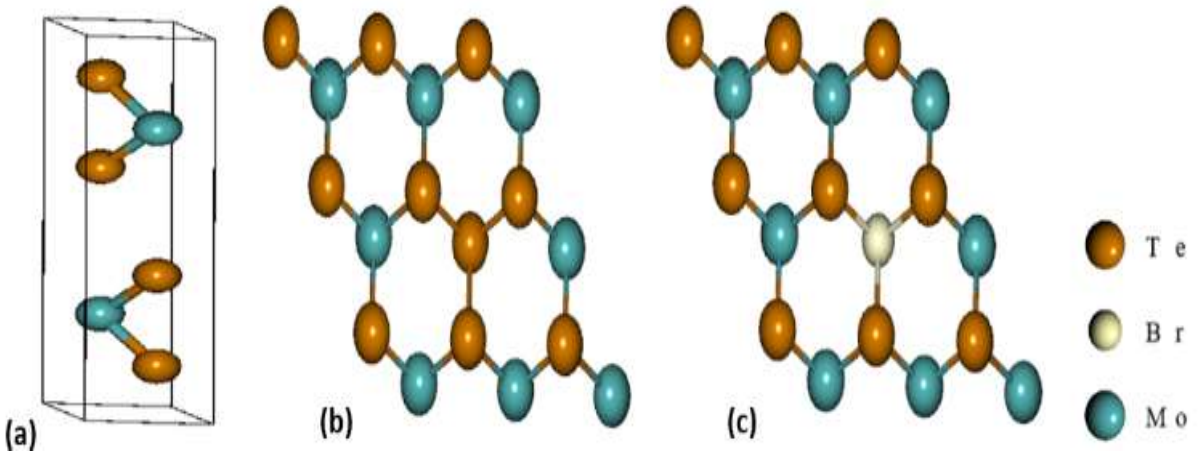

Fig. 1 (a) Bulk structure (b) Pristine (c) Br-doped $MoTe_2$ Monolayer

Here, two important and attractive configurations for $MoTe_2$ monolayer-based high-efficiency PSCs were proposed, opening useful research work for designing and fabricating low-cost and efficient PSCs. One-dimensional solar cell and capacitor simulation software was used as employed[30, 31]. Among the two structures, the $MoTe_2$ monolayer ETL demonstrated significant performances and Glass/FTO/Br-$MoTe_2$/$MAPbI_3$/Spiro-OMeTAD/Au was the best device with optimized performance parameters as PCE of 21.31%, Voc of 1.184 V, Jsc of *22.*504 mA/cm^2 and FF of 79.931%

The writing is organized as follows: the introductory section was followed by the design and simulation methodology section (section II), which gives a full description related to simulation methods. Section III presents the results and discussion, which show the influence of pure, and Bromine-doped $MoTe_2$ monolayer ETL in $MAPbI_3$-based solar cells. The conclusion section provides a summary of the

research findings as well as information on its future outlook.

II. METHODOLOGY

A. Model and Computational Summary

Quantum ESPRESSO an open-source simulation code [32] have been employed, using a plane wave basis set, based on the state-of-the-art density-functional theory (DFT). The ion cores and valence electrons interactions are treated by projector augmented wave (PAW) potentials by using 320 eV energy cut-off. The exchange-correlation potential was treated by Pardew-Burke-Ernzerhof parameterized generalized gradient approximations (PBE-GGA) [33] with the inclusion of full spin-orbit coupling (SOC). A 3x3 $MoTe_2$ monolayer supercell comprising Mo, Te and only one substituted dopant is employed for the calculations. A vacuum space of 15 Å along the z-axis direction is introduced to prevent the interlayer interactions [34]. For electronic iterations, the energy convergence threshold is set to be 10^{-5} eV. Broyden-Fletcher-Goldfarb-Shannon (B.F.G.S.) algorithms are used to fully optimize all the geometries until the Hellmann Feynman forces become less than 0.001eV /Å for each atom. The Brillouin zone was sampled according to the scheme proposed by Monkhost-Pack [35] with a high-density in-plane 12x12x1 k-point grid with 400 k-points.

Optical properties of these systems are investigated by using Yambo code which utilizes the quantum espresso outputs as input.

B. Design of Perovskite Solar Cell

The device simulation code used in this work is solar cell capacitance simulator (SCAPS-1D) version 3.3.10, developed at the University of Ghent Department of Electronics and Information System (ELIS), Belgium [3, 6, 37]. This software is among the best codes used for solar cell simulation [36]. SCAPS-1D solves the semiconductor equations, Poisson's equation, and the hole and electron continuity equations which are based on drift-diffusion transport, the software solves these three combined partial differential equations numerically for the electrostatic potentials' electron and hole concentrations as a function of positions. The device is simulated using the AM 1.5G spectrum with an incident power density of 1000 W/cm^2 and frequency of 1.0 x 10^{12} Hz.

Fig. 2a shows the diagram of the solar cell design. It is a typical n-i-p structure of PSC synthesised on fluorine tin oxide (FTO) coated glass substrate. The $CH_3NH_3PbI_3$ or Methyl ammonium lead triiodide ($MAPbI_3$) layer is sandwiched between hole transport and electron transport layers. In this work the HTL is spiro-OMeTAD and 2D-$MoTe_2$ as ETL, FTO serves as the front contact and Au acts as the back contact of the devices (Fig. 2a). The performance is compared with the experimental work of [23], who uses a 2D TiS_2, a member of TMDCs family as ETL in planer PSC (Glass/FTO/TiS_2/$MAPbI_3$/ spiro-OMeTAD/Au) while all other materials are the same with our design. Fig. 2b provides the procedural stages used for running the simulations.

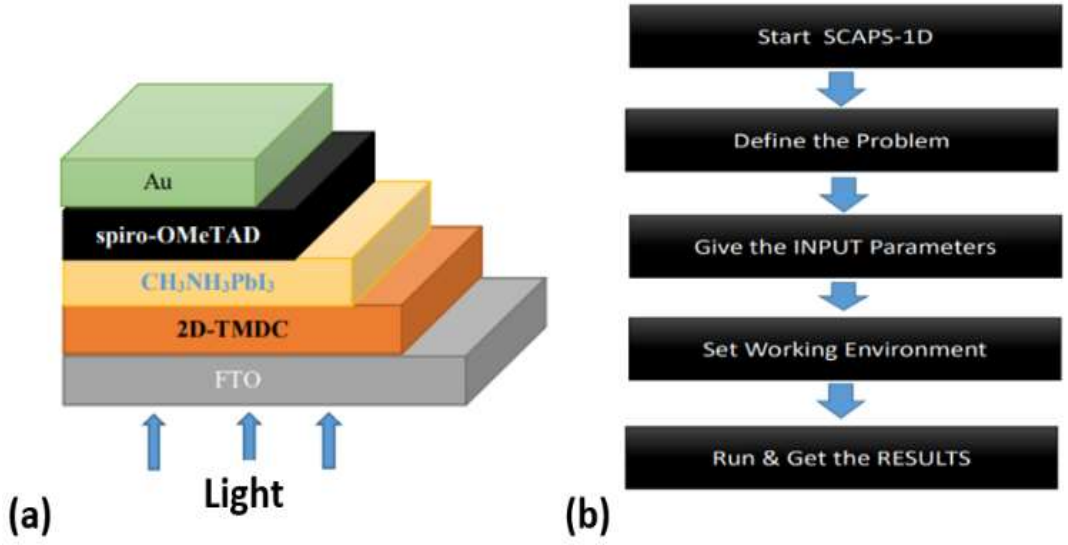

Fig. 2 (a) Schematic diagram of the device (b) Simulation procedure

Table I Material parameters used in the modelling of 2D-$MoTe_2$ ETL.

Parameters	FTO	Pure $MoTe_2$	Br-$MoTe_2$	$MAPbI_3$ [23]	spiro-OMeTAD [3]
Thickness (μm)	0.05	Varied	Varied	Varied	Varied
Band gap (eV)	3.5	1.01	1.21	2.25	2.88
Electron affinity (eV)	4.0	3	3.2	4.1	2.05
Relative permittivity (ε_r)	9.0	7.20	8.58	10.7	3
DOS Conduction Band (N_c) (cm^{-3})	2.2 x10^{18}	1.8 x10^{19}	2.2 x10^{18}	2.0 x10^{18}	2.0 x10^{18}
DOS valence Band (N_v) (cm^{-3})	1.8 x10^{19}	1.8 x10^{19}	2.2 x10^{18}	2.0 x10^{18}	1.8 x10^{19}
Electron mobility (cm^2/Vsec)	20	40	45	2	2x10^{-4}
Hole mobility (cm^2/Vsec)	8	21	20	2	2x10^{-4}
Donor concentration N_D (cm^{-3})	3	4	2	0	0
Acceptor concentration N_A(cm^{-3})	0	0	0	1 x10^9	2.0 x10^{19}
Defect density N_t (cm^{-3})	1x 10^{15}	1x 10^{15}	1x 10^{15}	1x 10^{15}	1.0 x10^{15}

III. RESULTS AND DISCUSSIONS

A. Electronic properties

The electronic properties of the $MoTe_2$ monolayer are calculated using GGA-PBE with the inclusion of relativistic spin-orbit coupling (SOC) due to its performance in predicting the band gap [38] in 2D-$MoTe_2$. The calculated band structure indicates that the materials are n-type semiconductors since the fermi level is closer to the conduction band minima than the valence band maxima [34] in the pure and doped structures. The band gap (E_g) is 1.01 and 1.21 eV for the pure and doped compounds respectively. From the corresponding band structures, the effective masses of electrons and holes were calculated using [20]

$$m^* = \pm\hbar^2\left(\frac{\partial^2 E}{\partial k^2}\right)^{-1} \quad (1)$$

Where m* is effective mass, $\hbar = \frac{h}{2\pi}$, h is planks constant, E is total energy corresponding with the wavevector and k is the wavevector of the particle. The band gap and the effective masses (in mass of electron unit (m_o)) are listed in Table II. From the effective masses, the conduction band effective density of states (N_c) and valence band effective density of states (N_v) were calculated for the doped and undoped $MoTe_2$ monolayers which are all presented in Table I.

Table II Calculated band gap energy, effective mass of electron and hole of pure and Br-doped $MoTe_2$ monolayers.

Compound	Eg (eV)	m^*_e/m_o	m^*_h/m_o
$MoTe_2$	1.02	0.175	-0.196
Br-$MoTe_2$	1.21	0.911	-0.839

B. Optical properties

It is essential for an ETL material which is a window layer to have high transmission in the visible light spectrum [39]. The optical properties of pure and Br-doped $MoTe_2$ monolayers are calculated using GGA-PBE with the inclusion of full relativistic spin-orbit coupling. These properties are often calculated from the dielectric function which is given by [40]

$$\varepsilon(\omega) = \varepsilon_1(\omega) + i\varepsilon_2(\omega) \quad (2)$$

Where ε_1 (ω) and ε_2 (ω) represent the real and imaginary parts of the dielectric tensor, respectively. The $\varepsilon_2(\omega)$ also describes the real transitions between the valence band and conduction band of the material. Here, we use the Kubo-Greenwood expression [41] given by (3).

$$\varepsilon_2(\omega) = \frac{2\pi e^2}{\Omega\varepsilon_o}\sum_{k,v,c}|\langle\Psi_k^c|u.r|\Psi_k^v\rangle|^2\,\delta(E_k^c - E_k^v - E) \quad (3)$$

To calculate $\varepsilon_1(\omega)$ from $\varepsilon_2(\omega)$, we use the Kramers-Kronig equation [18, 42] given by (4).

$$\varepsilon_1(\omega) = 1 + \left(\frac{2}{\pi}\right)\int_0^\infty d\omega' \frac{\varepsilon_2(\omega')\omega'}{\omega'^2 - \omega^2} \quad (4)$$

The real part and the imaginary are plotted in Fig. 3a and b respectively. Using the real and imaginary parts of epsilon, the values of the transmission coefficient (T) at the corresponding energies were calculated. The plot of the transmission coefficient against energy (Fig. 4c) shows that there is significant transmission of incoming photons of energies above the direct transition energy value for the considered materials, it also gives a very clear picture of the photon energies which are most likely to be transmitted by pure and Br-doped $MoTe_2$ monolayers, and this could be useful in the design of a suitable PSC ETL material.

Table III Calculated static relative dielectric permittivity ε (0) static transmission T (0), and static reflectivity coefficient of pure and Bromine $MoTe_2$ monolayers for x-polarization direction

Compound	ε (0) E‖x	R (0) E‖x	T (0) E‖x
$MoTe_2$	7.20	0.21	0.79
Br-$MoTe_2$	8.58	0.24	0.76

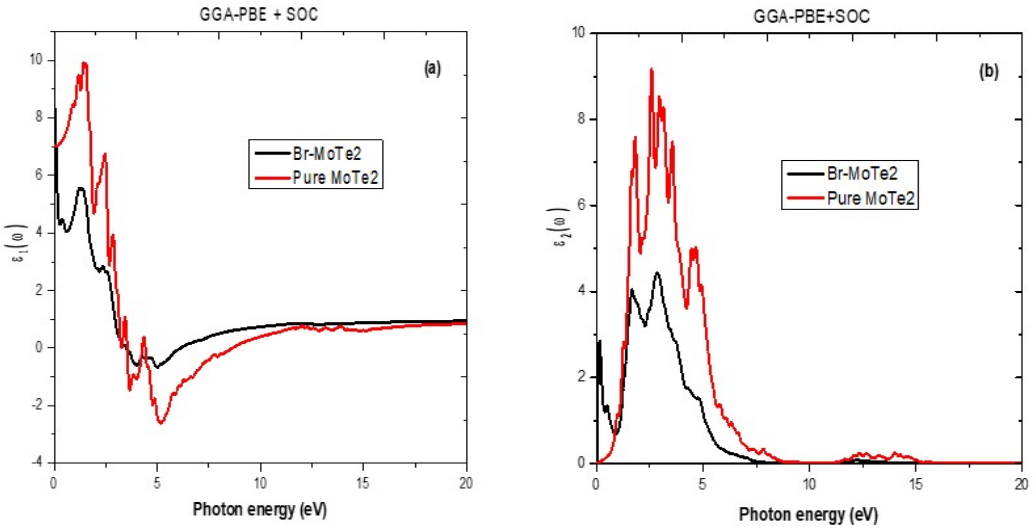

Fig. 3 Plots of (a) real, and (b) imaginary dielectric tensor of pure and Br-doped $MoTe_2$ monolayers.

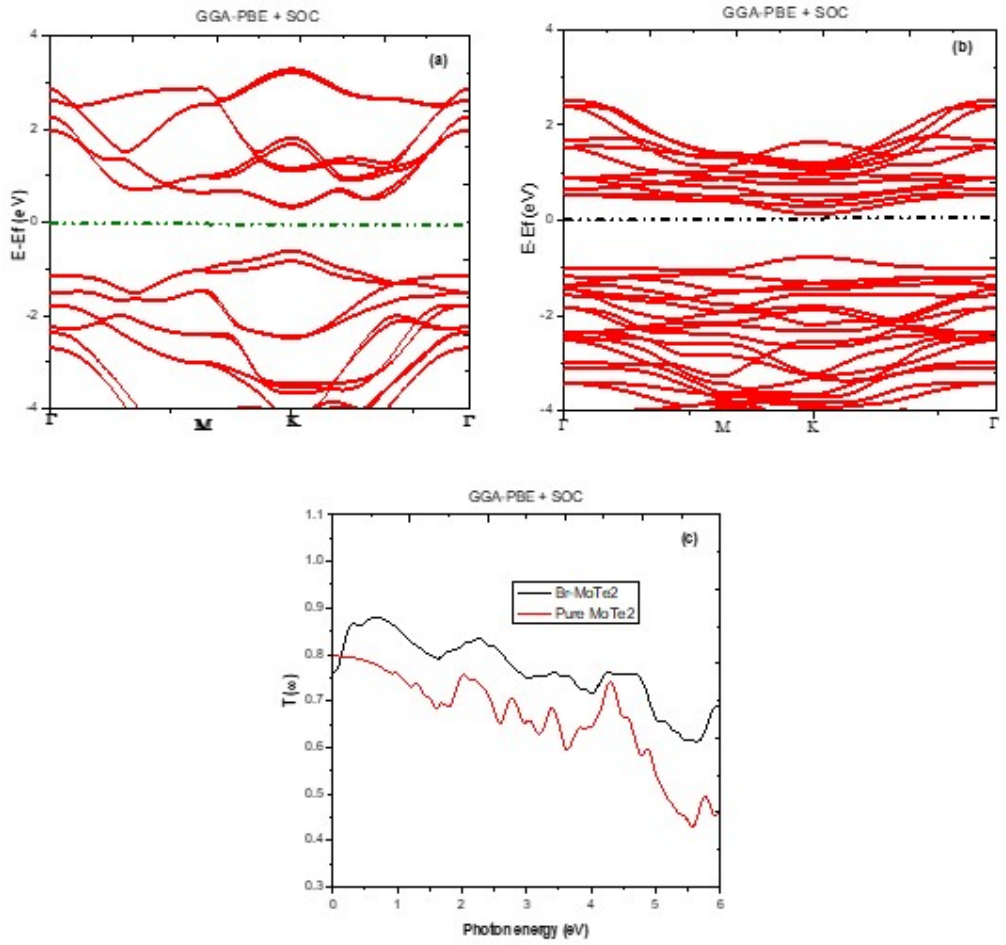

Fig. 4 Plots of (a) Band structure of pure, (b) Band structure of Br-doped and (c) Transmittance of pure and Br-doped $MoTe_2$ monolayers

C. Performance of the Devices.

The simulations were carried out based on the listed parameters collected from our materials simulations performed using DFT implemented in Quantum espresso code and experimental data source. Each layer of the perovskite solar cell has a very important role in the device's performance. Two different electron transport layers have been used in the device configuration of Glass/FTO/ETL/ $MAPbI_3$/spiro-OMeTAD/Au keeping all other parameters constant. The variation will help in getting the best-performing ETL among the two tested materials. Fig. 5 presents the J-V characteristics of the simulated PSC with the corresponding QE Plots of the PSC with different ETL, which is consistent with the J-V plots. Fig. 6 shows the J-V characteristics and quantum efficiency (QE) of the optimized device. QE covers the visible region of the solar spectrum. Br-doped $MoTe_2$ ETL-based solar cell has the maximum QE of 92.27%. It is rightly observed that the model with bromine doped shows better performance than its counterpart. The performance parameters obtained from the simulations are displayed in Table IV. The high performance of the perovskite solar cells with this material as an ETL layer could be attributed to the high mobility/conductivity of this n-type semiconductor, and the conduction band minimum of the material is in good alignment with the lower unoccupied molecular orbital (LUMO) of the active perovskite absorber layer. Based on the overall performance, Br-$MoTe_2$ has been used as the ETL for further investigations. We investigated the effect of ETL, absorber and HTL thicknesses and interface defect density at ETL/absorber on the performance parameters of the device.

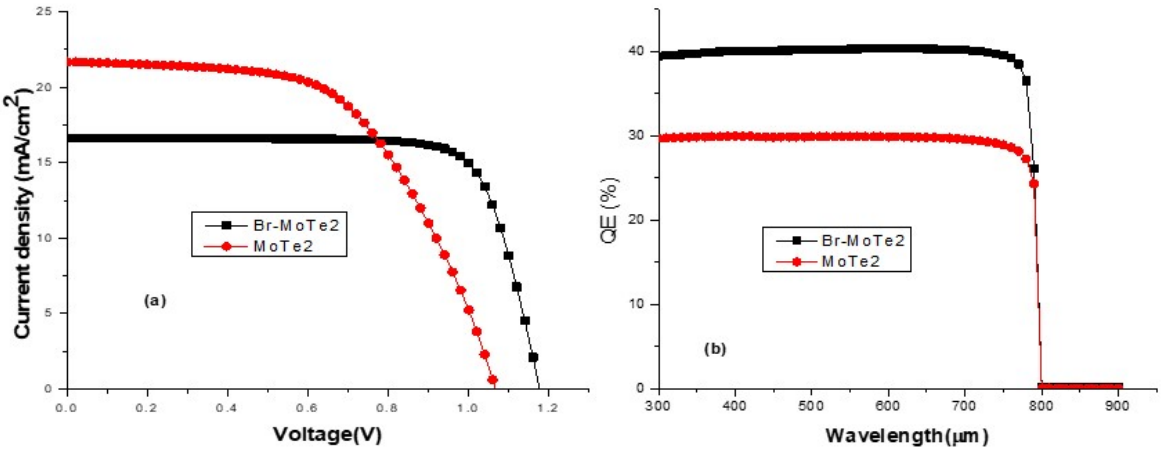

Fig. 5 (a) J-V characteristic, and (b) corresponding QE spectra of PSCs with different ETLs without optimization.

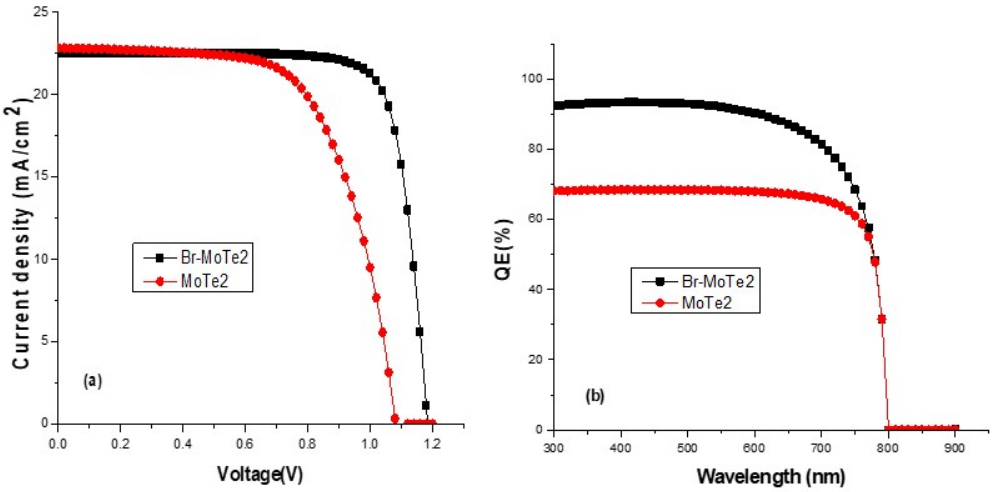

Fig. 6 (a) J-V characteristic, and (b) corresponding QE spectra of PSCs with different ETLs with optimization.

Table IV performance parameters of the device with various ETLs.

Performance Parameters	Unoptimized		Optimized	
	$MoTe_2$	Br-$MoTe_2$	$MoTe_2$	Br-$MoTe_2$
V_{oc}(V)	1.057	1.173	1.067	1.184
FF (%)	55.027	69.873	56.720	79.931
Jsc (mA/cm^2)	21.958	16.191	21.678	22.504
PCE (%)	12.778	13.281	13.121	21.310

D. Effect of ETL Thickness on the performance of the device

The electron transport layer plays a very essential role in determining the performance of PSC. 2D Br-doped $MoTe_2$ have been used in the device configuration Glass/FTO/Br-$MoTe_2$/$MAPbI_3$/spiro-OMeTAD/Au keeping all other material parameters the same. This helps in finding the efficiency of the materials as electron transport material in the device structure. Fig. 6 depicts (a) J-V characteristic, and (b) corresponding QE spectra of PSCs after optimization.

Optimization of ETL can control the charge recombination rates in perovskite solar cells. Fig. 7a shows the plots of performance parameters as a function of ETL thickness that is varied in the range of 0.001–0.01 µm. it can be observed that there is a significant decrease in Voc, Jsc and PCE as the layer thickness increases. This may be due to the increase in the recombination and fractional absorption of the ETL material in the device. The optimized ETL thickness is 0.001 µm giving a PCE of 21.304%, FF of 78.034%, Voc of 1.171V and Jsc of 23.308 mA/cm^2 (see Table V).

E. Effect of Absorber Thickness on the Performance of the Devices

The absorber layer, being the active layer in the device is very important, it absorbs solar radiation and converts it into electrons and holes [43]. Its thickness determines the amount of photogenerated excitons. Therefore, the thickness was varied with the performance parameters of the cell. The thickness of the absorber layer was varied from 0.1 µm to 1.0 µm (Table VI). Jsc, Voc and PCE of the device increase significantly with the increase of perovskite layer thickness [44]. The excitons produced due to photons absorption can cross the barrier potential that is the depletion layer which may result in higher Jsc, Voc and PCE, when the absorber layer becomes thicker (around 0.6 µm) the V_{OC}, J_{SC} and PCE remain constant (Fig. 7b). The optimized absorber thickness is 0.9 µm giving a PCE of 22.718%, FF of 78.574%, Voc of 1.185 V and Jsc of 24.388 mA/cm^2 (see Table V).

Table V J-V characteristics with the variation thickness of ETL.

Thickness (µm)	PCE (%)	Voc (V)	Jsc (mA/cm^2)	FF (%)
0.001	21.3041484	1.171303	23.30816	78.03457
0.002	21.1060705	1.170707	23.10316	78.03469
0.003	20.9279762	1.170443	22.90015	78.07980
0.004	20.7530349	1.170209	22.69904	78.12868
0.005	20.5796919	1.169978	22.49984	78.17750
0.006	20.4078377	1.169747	22.30252	78.22604
0.007	20.2374483	1.169516	22.10705	78.27425
0.008	20.0685103	1.169285	21.91343	78.32214
0.009	19.9098974	1.169054	21.72162	78.40470
0.010	19.7437158	1.168824	21.53163	78.45183

Table VI J-V characteristics with the variation thickness of Absorber.

Thickness (µm)	PCE (%)	Voc (V)	Jsc (mA/cm^2)	FF (%)
0.1	10.3906	1.166852	10.73113	82.9811
0.2	15.73204	1.177393	16.30993	81.92402
0.3	18.64837	1.181607	19.46445	81.08222
0.4	20.31639	1.183667	21.33783	80.43905
0.5	21.31076	1.184728	22.50404	79.93187
0.6	21.91378	1.185266	23.26189	79.47973
0.7	22.30483	1.185509	23.77379	79.13993
0.8	22.5566	1.185572	24.13129	78.84331
0.9	22.71814	1.185522	24.38834	78.57437
1.0	22.81917	1.185397	24.57784	78.32358

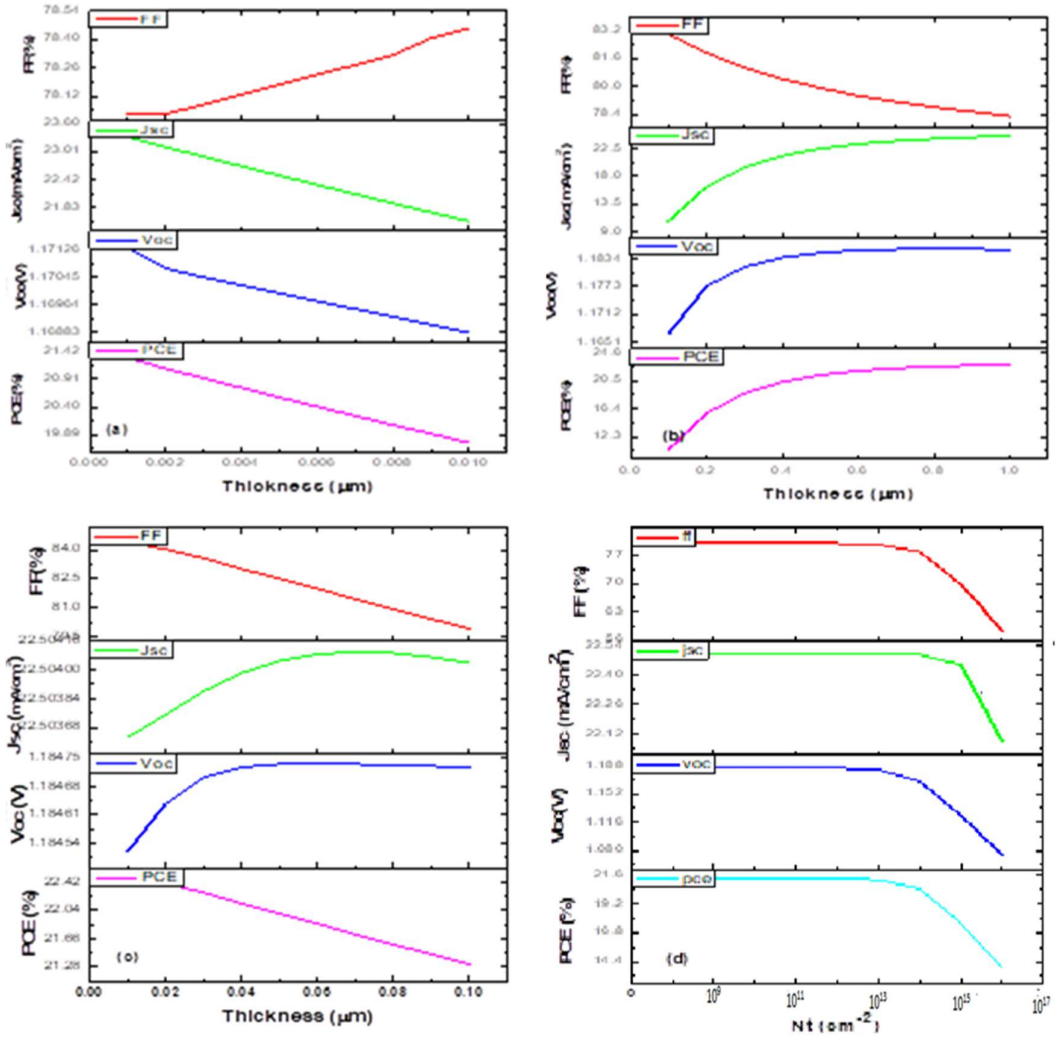

Fig. 7 Variation of performance parameter (V_{OC}, Jsc, FF and efficiency) of PSC with different, (a) ETL thickness, (b) perovskite thickness, (c) HTL layer thickness, and (d) Interface defect (ETL/$MAPbI_3$).

F. Effect of HTL Thickness on the Performance of the Devices

HTL extracts holes from the active absorber layer, transports them to the anode, and at the same time blocks electrons from reaching the anode. Varying the thickness of HTL is a promising technique to optimize the performance of PSC [45]. Fig. 7a and (Table VII) depict the performance parameters of the device with varying HTL thickness from 0.01 to 0.1 µm under illumination. Our findings reveal that PCE and FF decrease linearly with thickness while Voc and Jsc have no significant effect on the performance of the device as the thickness increases. The optimized HTL is 0.1 µm, PCE = 21.715%, FF = 81.447%, Voc = 1.184 V and Jsc = 22.504 mA/cm^2.

Table VII J-V characteristics with the variation thickness of HTL.

Thickness (µm)	Jsc (mA/cm^2)	Voc (V)	FF (%)	PCE (%)
0.01	22.50363	1.18452	84.38402	22.4934
0.02	22.50375	1.184637	84.02558	22.4002
0.03	22.50388	1.184701	83.56808	22.27957
0.04	22.50398	1.184735	83.01166	22.1318
0.05	22.50405	1.184735	82.50898	21.99799
0.06	22.50409	1.184736	82.00797	21.86447
0.07	22.50410	1.184734	81.44785	21.71512
0.08	22.50409	1.184732	80.93983	21.57962
0.09	22.50407	1.18473	80.43762	21.44567
0.10	22.50404	1.184728	79.93187	21.31076

Table VIII J-V characteristics parameters with varied ETL-Absorber defect density.

N_t (cm^{-2})	PCE (%)	Voc (V)	Jsc (mA/cm^2)	F (%)
10^9	21.31077	1.184728	22.50404	79.93189
10^{10}	21.31076	1.184728	22.50404	79.93187
10^{11}	21.31066	1.184725	22.50404	79.93165
10^{12}	21.30966	1.184703	22.50403	79.92945
10^{13}	21.29968	1.184476	22.50398	79.90747
10^{14}	21.19098	1.182316	22.5035	79.64661
10^{15}	20.43282	1.167227	22.49864	77.80663
10^{16}	17.62303	1.124423	22.45153	69.80794
10^{17}	13.91549	1.074333	22.08722	58.64333

G. Effect of Interface Defect Density at ETL/MAPbI3 on the Performance of the Devices

Due to the structural discontinuity in solar cells, defect states are often found between two-layer interfaces, they lead to photogenerated current loss. The impact of defect interface density is mostly expressed in terms of minority carrier recombination velocities [46, 47]. To explore the influence of the interface defect on the 2D-$MoTe_2/CH_3NH_3PbI_3$ interface of PSCs, the N_t was varied from 10^9 to 10^{17} cm^{-2} while keeping other parameters constant. Fig. 7d shows the performance parameters varied with interface defects density of 2D Br-$MoTe_2/CH_3NH_3PbI_3$. From the results (Table VIII) obtained, the photovoltaic parameters (PCE, FF, Jsc, and Voc) are not affected by the defect density for the range 10^9 to 10^{13} cm^{-2}. Beyond 10^{13} cm^{-2}, all performance parameters decrease with increasing Nt. This could be because of the recombination at the interface. Hence, the interface modification and film morphology to control N_t must be carefully regulated when fabricating PSCs with high efficiency [36]. The optimized interface defect is 10^9 cm^{-2} with a PCE of 21.310%, FF of 79.931%, Jsc of 22.504 mA/cm^2 and Voc of 1.184 V (Table VIII).

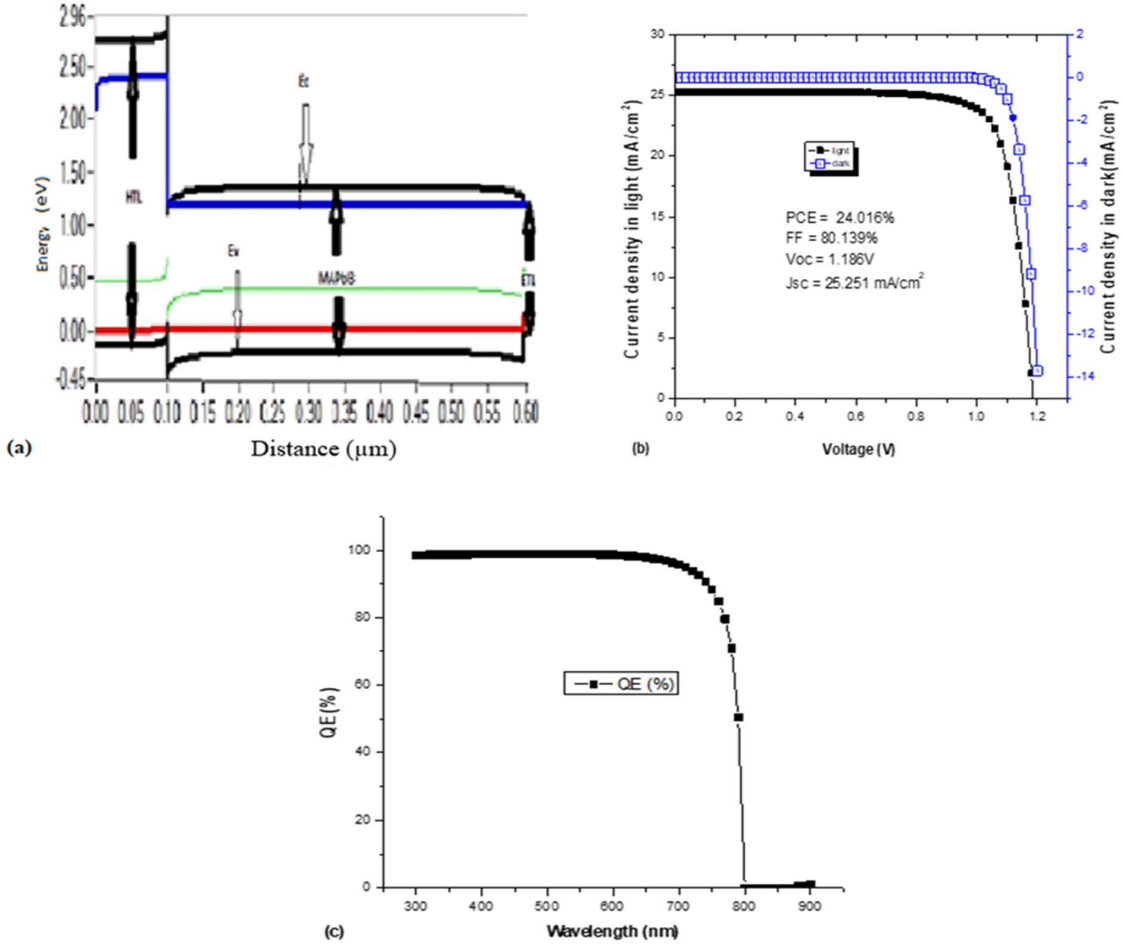

Fig. 8 (a) Energy band diagram (b) The optimized J-V curve under illumination and in the dark and (c) QE plot of the optimized device.

H. Performance of the optimized PSC

After obtaining the optimized ETL (0.001 µm), absorber (0.9 µm) HTL (0.07 µm) thicknesses and the interface defect density (10^9 cm^{-2}) for Br-doped $MoTe_2$ monolayer devices, we then run a final simulation with the optimal parameters. The results yielded a PCE of 24.01%, J_{sc} of 25.251 mA/cm^2, V_{oc} of 1.186 V, and FF of 25.251% for Br-doped $MoTe_2$ monolayer ETL-based perovskite solar cell. These results are compared with the experimental results of Huang et al [48] who use TiS_2 2D TMDC (Table IX). There is appreciable improvement in the PCE of the device. Fig. 8 shows the energy band diagram and J-V characteristic for dark and illumination conditions and the QE plot (max 98%) of the optimized cell.

Table IX Performance comparison between $MoTe_2$ and TiS_2 monolayer ETLs in PSC.

ETM	Configuration	FF (%)	J_{sc} (mA/cm^2)	V_{oc} (V)	PCE (%)	References
Br-$MoTe_2$	FTO/$MoTe_2$/$MAPbI_3$/ spiro-OMeTAD/Au	80.139	25.251	1.186	24.016	This work
$MoTe_2$	FTO/$MoTe_2$/$MAPbI_3$/ spiro-OMeTAD/Au	56.720	21.678	1.067	13.121	This work
TiS_2	FTO/TiS_2/$MAPbI_3$/ spiro-OMeTAD/Au	71.00	23.38	1.05	17.37	Expt. [48]

IV. CONCLUSION

In conclusion, we incorporated pristine and bromine-doped $MoTe_2$ monolayers in $MAPbI_3$ perovskite-based solar cells as ETL layers after calculating their electronic and optical properties from the first principle. Further, we studied the impact of the materials on the photovoltaic characteristics in the SCAPS-1D framework. We have optimized different properties of the device, such as the layers' thicknesses and ETL/Absorber interface defect density for further improvement of the device's performance. It has been demonstrated that 2D-Br doped ETL could have potential in perovskite-based solar cells. However, a more reliable and cost-effective fabrication method for good-quality layers is needed to make 2D materials-based solar cells scalable and commercially viable. 2D-Br doped ETL has shown exceptional properties compared to its counterpart. The performance of the device gave V_{oc} = 1.186 V, J_{sc} = 22.251 mA/cm^2, FF = 80.139% and PCE = 24.016%. This result shows how monolayer $MoTe_2$ can serve as a suitable ETL material for perovskite solar cells.

ACKNOWLEDGEMENT

We thank all co-authors for their valuable contributions; we also acknowledge the help offered by the Department of Physics, Kaduna State University, Kaduna Nigeria, for the use of their computational laboratory.

CONFLICTS OF INTEREST

The authors declare that they have no known competing financial interests or personal relationships that could have appeared to influence the work reported in this paper.

References

[1] J. Bisquert, The physics of solar energy conversion, First edition. ed. Boca Raton: CRC Press, 2020, p. 1 online resource. [Online]. Available.

[2] S. Gorjian and A. Shukla, *Photovoltaic solar energy conversion: technologies, applications and environmental impacts*. London, United Kingdom; San Diego, CA, United States: Academic Press, an imprint of Elsevier, 2020, pp. x, 452 pages.

[3] A. K. Singh, S. Srivastava, A. Mahapatra, J. K. Baral, and B. Pradhan, "Performance optimization of lead free-MASnI3 based solar cell with 27% efficiency by numerical simulation," *Optical Materials,* vol. 117, p. 111193, 2021.

[4] W. Chu, X. Li, S. Li, J. Hou, Q. Jiang, and J. Yang, "High-performance flexible perovskite solar cells with a metal sulfide electron transport layer of SnS2 by room-temperature vacuum deposition," *ACS Applied Energy Materials,* vol. 2, no. 1, pp. 382-388, 2018.

[5] A. Di Carlo, A. Agresti, F. Brunetti, and S. Pescetelli, "Two-dimensional materials in perovskite solar cells," *Journal of Physics: Energy,* vol. 2, no. 3, p. 031003, 2020.

[6] A. Kheralla and N. Chetty, "A review of experimental and computational attempts to remedy stability issues of perovskite solar cells," *Heliyon,* vol. 7, no. 2, p. e06211, 2021.

[7] S. Rawat, N. Shrivastav, R. Pandey, and J. Madan, "Optimizing Photovoltaic Performance of MASnPbI3 Perovskite Solar Cells through Layer Thickness Variations," in *2023 IEEE Devices for Integrated Circuit (DevIC)*, 2023, pp. 38-41: IEEE.

[8] G. V. Sannino *et al.*, "Development of SnO_2 Composites as Electron Transport Layer in

Unencapsulated $CH_3NH_3PbI_3$ Solar Cells. Solids, vol. 2, pp. 407–419, 2021.
[9] N. A. Abd Malek *et al.*, "Ultra-thin MoS2 nanosheet for electron transport layer of perovskite solar cells," *Optical Materials,* vol. 104, p. 109933, 2020.
[10] Z. K. Wang and L. S. Liao, "Doped charge-transporting layers in planar perovskite solar cells," *Advanced Optical Materials,* vol. 6, no. 17, pp. 1800276, 2018.
[11] E. Danladi *et al.*, "Defect and doping concentration study with series and shunt resistance influence on graphene-modified perovskite solar cell: a numerical investigation in SCAPS-1D framework," *Journal of the Indian Chemical Society,* vol. 100, no. 5, pp. 101001, 2023.
[12] H. Tan *et al.*, "Efficient and stable solution-processed planar perovskite solar cells via contact passivation," *Science,* vol. 355, no. 6326, pp. 722-726, 2017.
[13] W. Yu *et al.*, "Breaking the bottleneck of lead-free perovskite solar cells through dimensionality modulation," *Chemical Society Reviews,* 2024.
[14] T. A. Berhe *et al.*, "Organometal halide perovskite solar cells: degradation and stability," *Energy & Environmental Science,* vol. 9, no. 2, pp. 323-356, 2016.
[15] M. Wu *et al.*, "Synthesis of two-dimensional transition metal dichalcogenides for electronics and optoelectronics," *InfoMat,* vol. 3, no. 4, pp. 362-396, 2021.
[16] E. Elahi *et al.*, "Contemporary innovations in two-dimensional transition metal dichalcogenide-based P–N junctions for optoelectronics," *Nanoscale,* 2024.
[17] X. Hu *et al.*, "Structural regulation and application of transition metal dichalcogenide monolayers: Progress and challenges," *Coordination Chemistry Reviews,* vol. 499, pp. 215504, 2024.
[18] A. Mohammed, A. Shu'aibu, S. G. Abdu, and M. M. Aliyu, "Two-dimensional pure and bromine doped $MoTe_2$ and WSe_2 as electron transport materials for photovoltaic application: A DFT approach," *Computational Condensed Matter,* pp. e00855, 2023.
[19] Y. C. Lin, R. Torsi, D. B. Geohegan, J. A. Robinson, and K. Xiao, "Controllable Thin-Film Approaches for Doping and Alloying Transition Metal Dichalcogenides Monolayers," *Advanced Science,* vol. 8, no. 9, pp. 2004249, 2021.
[20] S. Roy and P. Bermel, "Electronic and optical properties of ultra-thin 2D tungsten disulfide for photovoltaic applications," *Solar Energy Materials and Solar Cells,* vol. 174, pp. 370-379, 2018.
[21] Y. Chen, S. Yu, T. Jiang, X. Liu, X. Cheng, and D. Huang, "Optical two-dimensional coherent spectroscopy of excitons in transition-metal dichalcogenides," *Frontiers of Physics,* vol. 19, no. 2, pp. 23301, 2024.
[22] R. Singh *et al.*, "Perovskite solar cells with an MoS 2 electron transport layer," *Journal of Materials Chemistry A,* vol. 7, no. 12, pp. 7151-7158, 2019.
[23] G. Yin *et al.*, "Low-temperature and facile solution-processed two-dimensional TiS 2 as an effective electron transport layer for UV-stable planar perovskite solar cells," *Journal of Materials Chemistry A,* vol. 6, no. 19, pp. 9132-9138, 2018.
[24] D. Zhao *et al.*, "Four-terminal all-perovskite tandem solar cells achieving power conversion efficiencies exceeding 23%," *ACS Energy Letters,* vol. 3, no. 2, pp. 305-306, 2018.
[25] E. Danladi *et al.*, "Highly efficient, hole transport layer (HTL)-free perovskite solar cell based on lithium-doped electron transport layer by device simulation," *Emergent Materials,* vol. 6, no. 6, pp. 1779-1795, 2023.
[26] E. Danladi *et al.*, "Modeling and simulation of> 19% highly efficient PbS colloidal quantum dot solar cell: a step towards unleashing the prospect of quantum dot absorber," *Optik,* vol. 291, pp. 171325, 2023.
[27] M. Alzaid, "Recent progress in the role of two-dimensional materials as an efficient charge transport layer in perovskite solar cells," *International Journal of Energy Research,* vol. 45, no. 9, pp. 12598-12613, 2021.
[28] S. O. A. Ahmad *et al.*, "Application of two-dimensional materials in perovskite solar cells: recent progress, challenges, and prospective solutions," *J. of Mat. Chem. C,* vol. 9, no. 40, pp. 14065-14092, 2021.
[29] L. Guo, J. Han, and J. Wang, "Recent advances in enhancing the photodetector performance of 2D materials combining with organic thin films," *J. of Mat. Chem. C,* 2024.
[30] E. Danladi *et al.*, "Broad-band-enhanced and minimal hysteresis perovskite solar cells with interfacial coating of biogenic plasmonic light trapping silver nanoparticles," *Mat. Res. Inno.,* vol. 27, no. 7, pp. 521-536, 2023.
[31] F. B. Sumona *et al.*, "Optimization of Perovskite-KSnI3 Solar Cell by Using Different Hole and Electron Transport Layers: A Numerical SCAPS-1D Simulation," *Energy & Fuels,* vol. 37, no. 23, pp. 19207-19219, 2023.
[32] P. Giannozzi *et al.*, "QUANTUM ESPRESSO: a modular and open-source software project for quantum simulations of materials," *Journal of Physics: Condensed matter,* vol. 21, no. 39, pp. 395502, 2009.
[33] J. P. Perdew, K. Burke, and M. Ernzerhof, "Generalized gradient approximation made simple," *Physical review letters,* vol. 77, no. 18, pp. 3865, 1996.
[34] L. Chhana, R. C. Tiwari, B. Chettri, D. Rai, S. Gurung, and L. Zuala, "Ab initio investigation of non-metal-doped ZnS monolayer," *Applied Physics A,* vol. 127, no. 9, pp. 729, 2021.
[35] H. J. Monkhorst and J. D. Pack, "Special points for Brillouin-zone integrations," *Physical Review B,* vol. 13, no. 12, pp. 5188, 1976.

[36] E. Danladi, M. Kashif, A. Ichoja, and B. B. Ayiya, "Modeling of a Sn-Based HTM-Free Perovskite Solar Cell Using a One-Dimensional Solar Cell Capacitance Simulator Tool," *Transactions of Tianjin University,* vol. 29, no. 1, pp. 62-72, 2023.

[37] I. T. Bello *et al.*, "Thickness Variation Effects on the Efficiency of Simulated Hybrid Cu2ZnSnS4-Based Solar Cells Using SCAPS-1D," 2021.

[38] F. Mahajabin, M. R. Islam, M. M. Masud, and M. M. Rahman, "Role of compressive and tensile strains and spin-orbit coupling on structure and behaviours of cubic FAPbI3 perovskites: A first-principles prediction," *Materials Chemistry and Physics,* vol. 313, pp. 128763, 2024.

[39] M. Dhankhar, O. P. Singh, and V. Singh, "Physical principles of losses in thin film solar cells and efficiency enhancement methods," *Renewable and Sustainable Energy Reviews,* vol. 40, pp. 214-223, 2014.

[40] M. Roknuzzaman, J. A. Alarco, H. Wang, and K. K. Ostrikov, "Structural, electronic and optical properties of lead-free antimony-copper based hybrid double perovskites for photovoltaics and optoelectronics by first-principles calculations," *Computational Materials Science,* vol. 186, pp. 110009, 2021.

[41] A. Radzwan, A. Lawal, A. Shaari, I. M. Chiromawa, S. T. Ahams, and R. Ahmed, "First-principles calculations of structural, electronic, and optical properties for Ni-doped Sb2S3," *Computational Condensed Matter,* vol. 24, pp. e00477, 2020.

[42] S. A. Yamusa, A. Shaari, and I. Isah, "Structural stability, Electronic and Optical Properties of Bulk MoS_2 Transition Metal Dichalcogenides: A DFT Approach," *J. Appl. Phys,* vol. 14, pp. 40, 2022.

[43] S. Fonash, *Solar cell device physics*. Elsevier, 2012.

[44] T. M. Koh *et al.*, "Formamidinium tin-based perovskite with low E g for photovoltaic applications," *Journal of Materials Chemistry A,* vol. 3, no. 29, pp. 14996-15000, 2015.

[45] E. Danladi *et al.*, "Impact of hole transport material on perovskite solar cells with different metal electrodes: a SCAPS-1D simulation insight," *Heliyon,* vol. 9, no. 6, 2023.

[46] M. S. Rahman, S. Miah, M. S. W. Marma, and T. Sabrina, "Simulation-based investigation of inverted planar perovskite solar cell with all metal oxide inorganic transport layers," in *2019 International Conference on Electrical, Computer and Communication Engineering (ECCE)*, 2019, pp. 1-6: IEEE.

[47] O. M. Durodola, C. Ugwu, and E. Danladi, "Highly efficient lead-free perovskite solar cell based on magnesium-doped copper delafossite hole transport layer: a SCAPS-1D framework prospect," *Emergent Materials,* vol. 6, no. 5, pp. 1665-1684, 2023.

[48] P. Huang *et al.*, "Room-temperature and aqueous solution-processed two-dimensional TiS2 as an electron transport layer for highly efficient and stable planar n–i–p perovskite solar cells," *ACS applied materials & interfaces,* vol. 10, no. 17, pp. 14796-14802, 2018.